dc and high-frequency transport in quasi-one-dimensional quantum wires with rough boundaries

C. Lettau, M. Wendel, A. Schmeller, W. Hansen, and J. P. Kotthaus
Sektion Physik, Ludwig-Maximilians-Universität München, D-80539 München, Germany

W. Klein, G. Böhm, G. Tränkle, and G. Weimann
Walter Schottky Institut, Technische Universität München, D-85748 Garching, Germany

M. Holland
Department of Electronics and Electrical Engineering, University of Glasgow, GB-Glasgow G128QQ, United Kingdom
(Received 17 January 1994)

We fabricate quasi-one-dimensional electron wires by low-energy ion-beam exposure in $Al_xGa_{1-x}As/GaAs$ heterojunctions and study their transport properties in the low- and high-frequency domain. Typical widths of our electron wires range from 100 nm to 1 μm. The static and far-infrared (FIR) conductivities are measured at low temperatures ($T \leq 4.2$ K) and high magnetic fields ($B \leq 12$ T). The experiments demonstrate that in these wires a large proportion of the boundary scattering events is diffuse. The FIR conductivity exhibits intersubband and intrasubband plasmon resonances. The linewidths of these excitations reflect an intriguing anisotropy that arises from a mode-dependent sensitivity of these high-frequency excitations on the boundary roughness. Photoluminescence experiments indicate that the confinement is accompanied by creation of defects in the plane of the electron system that strongly reduce the mobility of the electrons in the areas exposed to the ion beam.

I. INTRODUCTION

For the fabrication and study of one- and zero-dimensional electron systems the high-mobility two-dimensional electron system (2DES) in modulation-doped $Al_xGa_{1-x}As/GaAs$ heterojunctions is preferentially used. A variety of techniques has been employed to induce the lateral confinement potentials that form one- and zero-dimensional electron systems out of the 2DES.[1] At present, in the most widespread techniques either patterned field-effect electrodes are employed or material is removed from the crystal surface by various etching techniques.[2] Electron systems patterned with these techniques are found to have relatively long lateral depletion lengths, i.e., the pattern prepared on the sample surface is larger than the geometry of the electron system defined beneath. For example, in narrow wires defined beneath the gap of a split gate the electron channels have a much smaller width than the gap.[3-7] As a consequence the confinement potential induced by charges on the gate electrodes or on the etched crystal surface—the so-called bare confinement potential—is rather smooth. This has important implications on electronic properties, like e.g., the character of boundary scattering processes, i.e., how electron trajectories are reflected at the edge of the electron channels. The channel boundaries are smooth in the sense that the boundary roughness is of long range in comparison to the Fermi wavelength and thus scattering processes are predominantly specular, i.e., the momentum along the channel is conserved. Short-range roughness as induced, e.g., by ion damage techniques, on the other hand, can provide large momentum transfer along the channels and, correspondingly, scattering at the channel edge is largely diffuse.[8-11]

After a brief description of the sample preparation in Sec. II we would like to review in Sec. III characteristic features of the magnetotransport properties of ion-beam-defined electron wires demonstrating the diffuse character of boundary scattering processes in these wires. In Sec. IV we present measurements of the far-infrared (FIR) conductivity in arrays of electron wires fabricated by the same technique. In our FIR transmission experiments we employ a metallic grating coupler oriented perpendicular to the electron wire array so that not only intersubband plasmons with wave vector $q=0$ but also intrasubband plasmons with $q \neq 0$ along the wires are excited. Interestingly, the two different modes observed in the FIR exhibit very different linewidths. This can be understood in terms of a different sensitivity of the observed modes on the rough character of the wire boundary. Additional information about the confinement mechanism is obtained from photoluminescence studies presented in Sec. V. The photoluminescence spectra of ion-beam-irradiated quantum wells indicate that the irradiation with low-energy ions creates defects in the plane of the quantum well that severely deteriorate the carrier mobility. Thus the lateral confinement defined with low-energy ion beams is accompanied by a large reduction of the mobility in the irradiated areas. We suggest that this might be the origin of the strong boundary roughness found in the transport experiments.

II. EXPERIMENTAL NOTES

The preparation of our electron wires starts with the growth of modulation-doped high-mobility $Al_{0.3}Ga_{0.7}As/GaAs$ heterojunction wafers by molecular-beam epitaxy. For the experiments described in the following different heterojunction layers have been used

0163-1829/94/50(4)/2432(12)/$06.00

with electron densities ranging between $n_s = 3.7 \times 10^{15}$ m^{-2} and 5×10^{15} m^{-2} and mobilities between 17 m^2/Vs and 115 m^2/Vs at $T = 4.2$ K. The location of the heterojunction interface is typically 60 nm below the crystal surface; specific numbers will be given in the discussion of the respective experiments. For the magnetotransport experiments Ohmic contacts are fabricated with Ni-AuGe evaporated through a polymethylmethacrylat (PMMA) positive resist mask and alloyed at 430 °C. Then a suitable resist mask pattern is generated for the ion-beam irradiation process forming the desired geometry of the electron system. The ion-beam irradiation results in a depletion of mobile electrons of the 2DES except from those areas protected by the mask. The resist layers used for the protecting mask consist either of a 100-nm-thick electron sensitive negative resist (Hoechst AZ PN 114) or of a 150-nm-thick positive photoresist layer (Shipley AZ1805, thinned 1:1). The resist patterns are created by electron-beam lithography or holographic lithography, respectively.

The static magnetotransport of ion-beam-defined quantum wire is studied on single wire structures. The irradiation masks for these samples are created by electron-beam lithography. The geometry of our devices is illustrated in the inset of Fig. 1(a). Here, the Ohmic contacts are interconnected by single negative resist stripes forming wires and voltage probes. We have used resist stripes of widths between 100 and 1000 nm. Three pairs of opposing voltage probes for measurements of the Hall resistance and the longitudinal resistance are arranged along the wires with 7.5 μm separation between each pair.

For the studies of the high-frequency conductivity by FIR transmission measurements, we have to use large arrays of periodically repeated quantum wires covering an area of typically $(2\ mm)^2$. We define these multiple quantum wire arrays with a resist mask created by exposure to a holographic light pattern. Periods of the wire arrays are 500 and 700 nm. The widths of the photoresist stripes are typically 40% of the period.

After fabrication of the resist mask the sample surface is exposed to the low-energy ion beam in order to deplete those areas from mobile electrons that are not protected by the resist mask. This technique of isolation by irradiation with low-energy ions has been previously used very successfully for the preparation of quantum wires for magnetotransport investigations.[8,11–14] The static transport data presented below demonstrate that the characteristic properties of our wires are very similar to those found in Refs. 8 and 11. The ion-beam exposure of our samples is performed in a commercial ion-milling machine with a Kaufman-type ion source modified to use low ion-dose rates (typically 5–6 $\mu A/cm^2$) with low acceleration voltages (200–300 V). We use Ne ions because of the lower sputtering rates as compared to the rates observed with Ar ions.[13,15,16] On the other hand, we prefer Ne to He since we expect the lighter He ions to straggle over larger lateral distances causing a larger depletion width or even a reduction of the channel mobility. The low sputtering rate is verified with an atomic force microscope with which we measure the step height between a protected and an unprotected area of a crystal surface after ion-beam exposure. The layer thickness of the material that is removed from the unprotected crystal surface by sputtering is 2–3 nm after exposure with a typical Ne ion dose (3.5 mC/cm^2) necessary to pattern the elec-

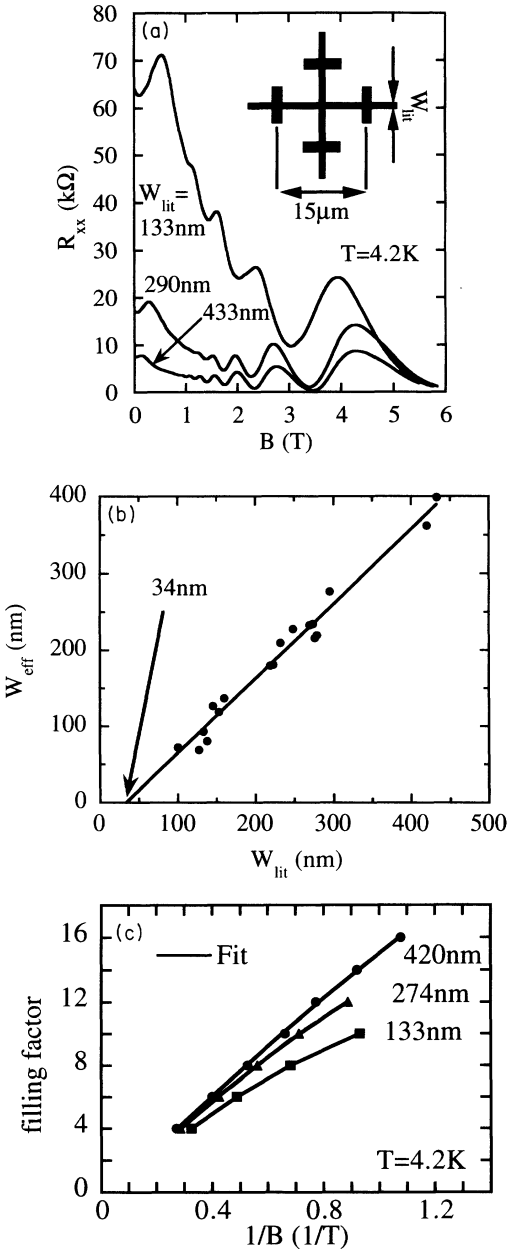

FIG. 1. (a) Longitudinal magnetoresistance of low-energy ion-beam-defined electron wires for different widths W_{lit} of the resist masks as indicated. The length of the wire between the voltage probes, with which the resistance is measured, is 15 μm. The inset shows the geometry of the sample. (b) The effective wire widths determined from the resistance maximum as described in the text versus the lithographic widths W_{lit} of the resist masks. (c) Fan charts of the magnetoresistance minima measured in wires with three different lithographic widths. The solid lines are fits to the data assuming a parabolic potential form with the 1D electron density and the subband spacing as parameters.

tron system. From the low sputtering rate we may already infer that the mechanism responsible for the lateral confinement in our samples is different from the one in devices fabricated by a conventional shallow etch. However, the mechanism that results in isolation of the sample areas exposed to a low-energy ion beam is still quite unclear.[12,16] The mean penetration depth of ions with a kinetic energy of 200–300 eV is calculated in Monte Carlo simulations to be far less than the distance of the electron system from the crystal surface.[17] However, it has already been suggested that channeling processes with corresponding higher penetration depths can be important.[18] The experimental results presented below substantiate the difference between the confinement potentials in low-energy ion-beam-defined wires and the ones defined by conventional wet or dry etching techniques. They also yield valuable information on the mechanism that removes mobile electrons from ion-beam-exposed areas of a heterojunction.

The irradiation effect on the 2DES is monitored *in situ* during the ion-beam exposure by a resistance measurement between two Ohmic contacts on a part of the crystal surface that is not covered with resist. However, at low temperatures the exposed parts of the sample become insulating well before the room-temperature resistance between the two Ohmic contacts saturates. Hence, we introduced additional criteria for the termination of the exposure process. The single wire structures for magnetotransport experiments were successively exposed to increasing ion doses until the voltage measured between Hall contacts at $B=0$ and low-temperature vanished. On the other hand, in the wire arrays for FIR transmission measurements the successful isolation of the wires is judged from the deviation of the measured FIR resonance frequency from the cyclotron resonance position. After recording the FIR transmission spectra the samples were exposed to an additional ion dose, if there was still resonant FIR absorption at the cyclotron frequency $\omega_c = eB/m^*$. Here we use $m^* = 0.07 m_e$ as the effective electron mass in GaAs. Typical irradiation doses for patterning range between 2 and 5 mC/cm^2.

In the FIR we want to study not only one-dimensional-(1D-) intersubband[19,20] but also 1D-intrasubband plasmons.[21] To be able to excite 1D-intrasubband plasmons with wave vector q along the wires we use a metallic grating coupler fabricated on the sample surface. Such a grating coupler was prepared on a number of ion-beam-defined wire arrays after they had been successfully characterized by investigation of the 1D-intersubband plasmon. The grating coupler consists of 35-nm-thick gold stripes arranged in an array of period $b=1$ μm with the grating stripes oriented perpendicular to the electron wires. Therefore it couples the transversal FIR radiation to the longitudinal one-dimensional plasmon mode with wave vector $q=2\pi/b$ along the wires. The aspect ratio between stripe width and period is about 0.7. Since the ion-beam exposure is hardly associated with material removal the crystal surface is smooth after definition of the electron wire array and the subsequent preparation of a microstructured metal pattern is done with relative ease as compared to previous experiments[21] on etched wire arrays. We note that the small surface corrugation makes this technique also very advantageous for combination with additional patterned front gates on the sample surface.

III. MAGNETOTRANSPORT IN SINGLE WIRE STRUCTURES

In the following we discuss the static magnetotransport properties of our single wire devices. In agreement with previous reports[8,11–14] these properties are distinct from properties of wires fabricated with more conventional methods. Namely, the lateral depletion length is found to be very small and a large proportion of the boundary scattering events is diffuse. In Fig. 1(a) we depict the longitudinal magnetoresistance measured at $T=4.2$ K on electron wires with typical widths of the resist stripes between $W_{\rm lit}=433$ and 133 nm. At magnetic fields below about $B=1$ T a pronounced magnetoresistance maximum is observed that reflects the effect of diffuse boundary scattering processes on the magnetotransport along the wire.[11] This can be understood qualitatively considering the effect of diffuse boundary scattering processes on classical electron trajectories propagating in the electron channel at different magnetic fields.[11] At zero magnetic field the channel resistance is predominantly determined by electron trajectories having a small number of collisions with the channel boundaries, i.e., trajectories that are reflected at glancing angles. A small magnetic field bends all trajectories towards the boundaries and thus intensifies contact with the channel boundaries. Diffuse scattering processes then lead to an enlarged resistance. At higher fields the opposing channel boundaries become decoupled, i.e., an electron trajectory is either bound to one of the boundaries or in the sample center. The resistance is now predominantly determined by edge states drifting along the boundaries, which in a classical picture correspond to skipping orbits. Diffuse boundary scattering processes can no longer prevent this drifting motion along the edges and, accordingly, the magnetoresistance decreases at high magnetic fields. The strength of the magnetoresistance anomaly indicates the importance of boundary roughness in our samples in correspondence with the results of other groups[11,22,23] as compared to wires defined by more conventional etching methods[24–28] or field-effect electrodes.[3,29]

From a classical analysis of this effect[11,30] it is found that the magnetoresistance maximum occurs at the magnetic-field strength at which the radius R_c of the classical cyclotron orbit of electrons at the Fermi energy is about two times the wire width: $W_{\rm eff} \approx R_c \times 0.55$. Here a square-well potential is assumed and scattering processes are assumed to be either specular or diffuse to a distinct degree. It is found that only the strength but not the position of the resistance maximum depends on the degree of diffuse scattering. This result has recently been confirmed by a more general quantum-mechanical transport calculation.[31] In Fig. 1(b) the effective width as determined from the resistance anomaly is plotted as a function of the lithographic width $W_{\rm lit}$ of the mask determined for inspection of the resist masks with a scanning electron microscope. The straight line is a least-squares

fit to the data with a slope of 0.98. The intercept with the abscissa reflects twice the sidewall depletion length, i.e., the amount by which the effective width of the electron channel is smaller than the lithographic width of the mask. We thus have a lateral depletion length smaller than 20 nm, a very low value compared to those found with other patterning techniques on $Al_xGa_{1-x}As/GaAs$ heterojunctions.[3,4,7,24,25,32–34] The slope of the line is close to one as is expected if the depletion length does not depend on the lithographic width.

At magnetic fields above 1 T the longitudinal magnetoresistance in Fig. 1(a) shows strong quantum oscillations. They arise from the magnetic depopulation of the one-dimensional subbands.[4] At small magnetic fields the density of states in quasi-one-dimensional channels strongly deviates from the density of states of two-dimensional Landau levels. Hence, the magnetoresistance oscillations deviate from the Shubnikov–de Haas (SdH) oscillations at small magnetic fields and their positions can thus be used to extract information on the lateral confinement. This is demonstrated in Fig. 1(c), where we depict the positions of the magnetoresistance minima for three wires with different lithographic widths. At small wire widths the positions clearly deviate from the linear $1/B$ behavior observed in two-dimensional systems, indicating one-dimensional confinement. If the effective confinement potential is assumed to be parabolic, the magnetic fields at which the subbands are depopulated can be determined analytically and compared to the experimental values.[4] From a fit to the data [solid lines in Fig. 1(c)] we obtain subband spacings of 0.4, 0.7, and 1.5 meV and 1D electron densities of 2.1×10^7, 1.4×10^7, and 5.4×10^6 cm^{-1} for the wires with the lithographic widths 420, 274, and 133 nm, respectively. The width of the potential at the Fermi energy is found in the parabolic model to be on average 1.5 times larger than the widths evaluated from the magnetoresistance anomaly in Fig. 1(b). The electronic widths determined by magnetic depopulation of the 1D subbands in our wires are equal to or larger than the corresponding lithographic widths determined by inspection with a scanning electron microscope. Hence, the assumption of a parabolic potential form leads to an unphysical result for the ion-beam-defined wires. For this reason, we use the effective wire widths $W_{\rm eff}$ determined by the resistance anomaly.

At sufficiently high magnetic fields the magnetic confinement dominates the electric confinement and the magnetoresistance oscillations do no longer deviate from the SdH period of the corresponding 2D electron system. Thus we can determine effective two-dimensional densities depicted as function of the effective wire widths in Fig. 2(a). The carrier density is found to be hardly dependent on the wire width except for the smallest wires investigated. Contrary to this behavior the electron density strongly decreases with the wire width in wires defined by more conventional techniques.[3,27,35]

The resistance at $B=0$ T, normalized to the electron density and the ratio between wire length and width, is used to determine an electron mobility in the wires. This mobility is depicted in Fig. 2(b) as function of the wire width. Solid and dashed-dotted lines are calculated with the assumption that the mobility in the wire is determined solely by the as-grown mobility of the initial heterojunction wafer material ($\mu=17$ m^2/Vs) and by the character of the boundary scattering processes. If the channel boundary scattering is 100% specular the mobility is the same as in the unprocessed wafer material independent of the wire width as indicated by the horizontal dashed-dotted line in Fig. 2(b). Including a dependence of the mobility on the electron density of the form $\mu \propto n_s^{3/2}$ in order to account for the reduced screening at lower densities[36] yields the dotted line. The figure shows that at least a 2D-screening model[36] does not suffice to explain the drastic mobility reduction observed in our ion-beam-defined wires. The full line below the data points represents the wire width dependence of the mobility for 100% diffuse boundary scattering processes calculated according to a model of Beenakker and van Houten.[10] The dashed line in Fig. 2(b) shows the mobility at $B=0$ T calculated in this model with the assumption that 50% of the scattering processes are diffuse. Comparison with the data indicates that the boundary scatter-

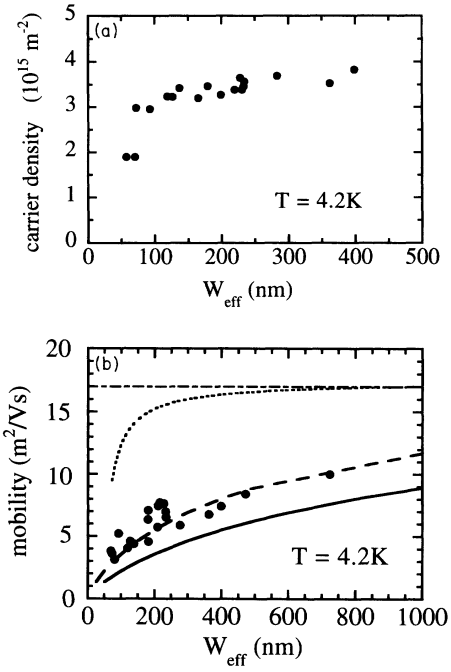

FIG. 2. (a) Effective two-dimensional carrier densities in low-energy ion-beam-defined quantum wires vs the effective wire widths. (b) Electronic mobility at $T=4.2$ K in the quantum wires of (a) determined from the resistance at $B=0$ T. The solid and the dashed lines are calculated assuming 100% and 50% diffuse scattering, respectively. The dashed-dotted line indicates the mobility with 100% specular boundary scattering. The dotted line represents a fit through the mobility values calculated from the experimental densities taken from (a) assuming 100% specular scattering and an explicit density dependence ($\mu \propto n_s^{3/2}$, see text). The electron wires in Figs. 1–4 are made from the same wafer material within an as-grown carrier density of 3.7×10^{15} m^{-2} and mobility of $\mu=17$ m^2/Vs at $T=4.2$ K. The heterojunction interface is 70 nm below the crystal surface.

ing is diffuse to a large degree.

Figure 3 shows the low-field longitudinal magnetoresistance recorded at different temperatures. The resistance anomaly arising from diffuse boundary scattering is reflected by the large maximum at $B=0.3$ T. Its position is temperature independent in the temperature range investigated ($T \leq 10$ K). From the maximum position we derive an effective wire width of 180 nm. At $B \leq 50$ mT a negative magnetoresistance is observed that becomes more pronounced at lower temperatures. It arises from weak localization of the electrons in the wires. As pointed out by Beenakker and van Houten weak localization in one-dimensional channels with widths smaller than the elastic mean free path is modified by the flux cancellation effect.[10] The weak-localization correction to the resistance is dependent on both the channel width and the character of the boundary scattering processes.[10] Assuming diffuse boundary scattering processes we can describe the magnetoresistance measured at $T=0.5$ K with the above wire width of 180 nm and a phase-coherence length of $l_\phi=0.65$ μm. Assuming specular boundary scattering processes we would derive a value of 1 μm for l_ϕ. With decreasing temperature we also observe that fluctuations of the magnetoresistance become more pronounced. These resistance fluctuations are reproducible as long as the sample remains at low temperatures. They are residues of the well-known universal conductance fluctuations in small devices.[9,37] From a theory[9] which takes into account the influence of boundary scattering on the magnitude of the fluctuations we can derive an additional value for the phase coherence length from the averaged low-field amplitude of these fluctuations. At $T=0.5$ K we thus derive $l_\phi=0.4$ μm. Comparison of this value for the phase coherence length with the value determined from the weak-localization correction above gives a further indication that the boundary scattering processes are diffuse.

Very interesting features are observable in the Hall resistance in both the low and the high magnetic field regimes. Investigations of the Hall effect in the regime of the quantized Hall effect are published elsewhere.[38] There we observe deviations from the Hall plateaus that

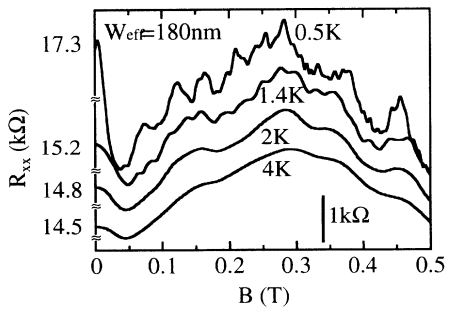

FIG. 3. Low-field magnetoresistance at different temperatures of an ion-beam-defined electron wire with an effective width of 180 nm. The traces are offset for clarity. The numbers at the left-hand side of the figure give the sample resistances at $B=0$ T.

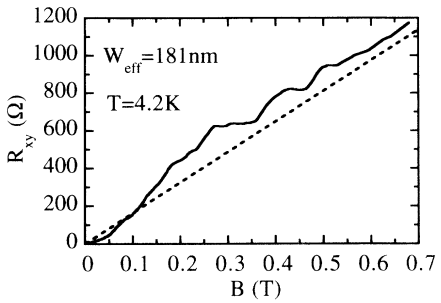

FIG. 4. Hall resistance of an electron wire with an effective width of 181 nm at low magnetic fields. The dotted line extrapolates the slope of the Hall resistance measured at high magnetic fields to $B=0$ T.

can be understood as a consequence of boundary-roughness-induced backscattering. Here we will focus on the low-field regime ($B<1$ T). In Fig. 4 the Hall resistance of a wire with an effective width of $W=181$ nm and voltage probes of similar dimension is shown. The widths of both the wire as well as the probes are only slightly broadened in the vicinity of their crossing as a result of proximity effects of the electron-beam lithography. The dotted line indicates the classical Hall resistance determined from extrapolation of the high-field data to low magnetic fields. The measured resistance clearly drops below the classical value at $B \leq 50$ mT. This so-called "quenching" of the Hall effect has first been observed by Roukes *et al.*[8] in ion-beam-defined wires and subsequently on various wire systems.[39,40] At a higher magnetic field the cyclotron radius becomes of the same order of magnitude as the radius of curvature of the channel boundary at the cross junction. Then the Hall resistance is strongly enhanced with respect to the classical value. This has also been previously observed and has been called the "last plateau."[8,39–41] Both effects are understood as a consequence of the ballistic motion of the electrons in the region of the crossing between wire and Hall probes.[42–44] Whereas at very low magnetic fields the electrons practically miss the Hall contacts they are focused into the contact when the cyclotron radius gets smaller. We would like to point out here that in the region where the Hall resistance is enlarged it exhibits a series of plateaulike features rather than a single one. They occur at magnetic fields which are about 1.4–2 times the value at which the first feature is observed. These observations have been reproduced on different cross junctions with different wire widths and broadenings. The strength of the features and their appearance as a plateau or a maximum is found to depend on the broadening of the cross junction. Recent numerical simulations by Geisel, Ketzmerick, and Schedletzky[45] assuming a cosine-shaped potential minimum in the center of the crossing predict very similar results. Depending on the depth of the minimum in the center and the radius of the corners the numerical calculations deliver two plateaulike structures in addition to the last plateau. The measured features are nearly temperature independent at $0.5 \leq T \leq 4.2$ K, which strongly supports the classical interpretation by Geisel, Ketzmerick, and Schedletzky.[45]

IV. FAR-INFRARED CONDUCTIVITY IN MULTIWIRE ARRAYS

The above-described static transport properties prove that the quality of our electron wires is very similar to the one of previous reports on ion-beam-defined wires. In particular, the results demonstrate that diffuse boundary scattering processes are important. In the following we would like to discuss the high-frequency conductivity in the FIR domain, which has not been investigated in ion-beam-defined wires previously. The FIR conductivity is measured by differential transmission spectroscopy[46] with a rapid scan Fourier-transform spectrometer at $T=2$ K. Two transmission spectra of the sample are subsequently recorded at different magnetic fields applied normal to the wire array such that the resonant absorptions of the electron system are at different frequencies. In the figures of the following discussions the relative transmission $T(B_1)/T(B_2)$ is shown, where the resonant absorption at magnetic field B_2 occurs at frequencies not shown in the figures.

We first discuss measurements on wire arrays with periods of 500 and 700 nm and no additional grating coupler on the sample surface. With the FIR radiation polarized perpendicular to the wires we excite the one-dimensional intersubband plasmon at wave vector $q=0$, the so-called dimensional resonance.[2,19] Since it arises from the collective motion of the electron system perpendicular to the wire boundaries the $B=0$ resonance frequency ω_0 is finite and only in high magnetic fields it gradually approaches the cyclotron resonance frequency. We used the deviation of the measured resonance position from the cyclotron resonance frequency ω_c according to the formula $\omega_{res}^2=\omega_0^2+\omega_c^2$ as a measure for successful ion-beam isolation of the wires. This formula is expected to be exact in case of a parabolic bare confinement potential and has been found to describe the magnetic-field dispersion of dimensional resonances in most[47] of the experimental wire systems fairly well.[2,48]

Transmission spectra of a wire array with period $a=500$ nm recorded at different magnetic fields at a temperature of 2 K are depicted in Fig. 5. The corresponding resonance positions and linewidths are depicted as functions of the magnetic field in Fig. 6. The sample has been exposed to an ion dose of 3 mC/cm^2 to define the electron wires. The light is polarized perpendicular to the electron wires. The resonance frequencies are significantly higher than the cyclotron frequency and the resonance linewidth drastically broadens with decreasing magnetic field. For instance, at $B=3$ T the resonance position is shifted to a frequency about 15 cm^{-1} higher than the cyclotron resonance position. The full width at half maximum (FWHM) of the resonance is 18.5 cm^{-1}, which is much larger than the value 2 cm^{-1} of the cyclotron resonance in the as-grown material. At magnetic fields below $B=1$ T no resonance can be resolved. Contrary to observations on wire arrays fabricated with other methods[19,49] the resonance oscillator strength decreases with decreasing magnetic field and does not depend significantly on the polarization of the radiation. In wire arrays with a period of 700 nm processed from the same

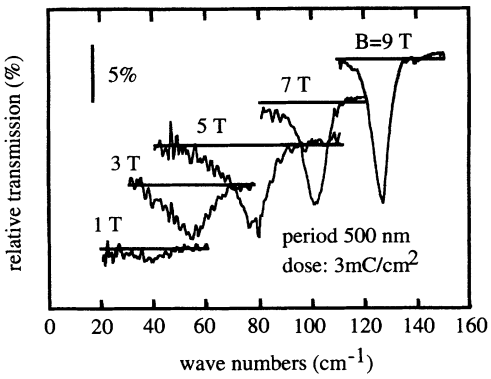

FIG. 5. Relative far-infrared transmission spectra recorded at $T=2$ K and different magnetic fields on an electron wire array with period $a=500$ nm defined by an ion-beam exposure of given dose. The cyclotron resonance linewidth of the as-grown heterojunction material from which this wire array was fabricated ranges between 2 and 3 cm^{-1} in the magnetic-field regime $1\le B\le 9$ T depicted. The samples in Figs. 5, 6, 8, and 9 are made from the same wafer material with an as-grown density of $n_s=5\times10^{15}$ m^{-2} and a mobility of 50 m^2/Vs at $T=4.2$ K. The heterojunction interface is located 55 nm beneath the crystal surface.

wafer material the resonance positions are very similar to the positions found in the 500 nm arrays. However, in the arrays with 700-nm period and a correspondingly larger wire width the resonance linewidth is significantly narrower. Here we find at $B=12$ T a FWHM of 2 cm^{-1} and it increases to 8 cm^{-1} at $B=2$ T. Furthermore, even at $B=0$ T a resonance is observed at 38 cm^{-1}, if the FIR light is polarized perpendicular to the wires. In the wire arrays with 700-nm period the oscillator strengths depend on the light polarization with respect to the wires. In perpendicular polarization the oscillator strength is roughly constant, in parallel polarization it decreases with decreasing magnetic field. This behavior is expected for 1D wire arrays and has been observed in previous measurements on samples patterned by more conventional methods.[19,49]

In electron wires generated by field-effect electrodes[19]

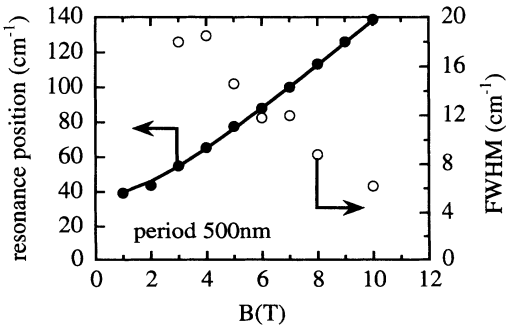

FIG. 6. Magnetic-field dependence of the resonance positions (filled circles) and FWHM (open circles) of the dimensional resonances of the sample in Fig. 5. The solid line is calculated according to $\omega_{res}^2=\omega_0^2+\omega_c^2$ with $\omega_0=37.5$ cm^{-1}.

or fabricated with more conventional etching techniques[20,49] the resonance linewidth often broadens slightly with decreasing magnetic field also. This broadening, however, is much less pronounced and is, as we believe, predominantly caused by fluctuations of the stripe width of the resist mask. We note that the resist masks used for the ion-beam exposure are prepared with the same technique as in those studies so that we exclude imperfections of the resist mask as an origin of the largely enhanced FWHM found in the ion-beam-defined wires. From Eq. (1), which will be used at the end of this section to describe intrasubband and intersubband plasmons, we see that at $B=0$ T the dimensional resonance frequency is proportional to $W^{-1/2}$, in case the wave vector q along the wires is zero.[50] From the observed FWHM $\Delta\omega_0$ of the resonance at $B=0$ T we thus can estimate a fluctuation ΔW of the wire width W by $\Delta W/W=2\times\Delta\omega_0/\omega_0$. In samples with period 700 nm we observe a $\Delta\omega_0/\omega_0$ of approximately 20%. Accordingly, the wire width fluctuation $\Delta W/W$ should be 40%, if the enhanced resonance linewidth was caused by inhomogeneous broadening. From inspection with the scanning electron microscope we can exclude that the irradiation masks have a fluctuation of this magnitude. However, we cannot exclude from the FIR-transmission measurements alone that the ion-beam definition itself creates wires with a width fluctuation causing an inhomogeneous broadening of the dimensional resonances.

On the other hand, the drastic increase of the resonance linewidths in ion-beam-defined wires at small magnetic fields can be understood in terms of diffusely scattering boundaries created by the ion-beam exposure. This is in qualitative agreement with the enhanced boundary roughness reflected by the magnetotransport properties in Sec. III. A simple argument considering the classical electron trajectories connected with the dimensional resonance shows that the damping of the dimensional resonance by diffuse boundary scattering decreases with increasing magnetic field. At $B=0$ the dimensional resonance is associated with electron motion perpendicular to the channel boundaries and the periodicity of the motion solely depends on how the electrons are reflected from those. If a sufficiently high magnetic field is applied perpendicular to the wires the classical electron trajectories become more cyclotronlike and the majority of them have reduced boundary contact. The magnetic field now localizes the wave function of an increasing number of electrons within the channel. Accordingly, the FWHM decreases with increasing magnetic field. The dependence of the lineshape on the wire width can be understood if we assume that the frequency of the oscillatory motion is determined by the potential shape within the wire. Since the external radiation field is effectively screened by the Coulomb field of the excited electron plasma, only a fraction of the electrons actually sense the boundary of the channel even at $B=0$. Therefore at small magnetic fields the resonances in narrower wires have a larger linewidth.

Our interpretation of the linewidth behavior as a special signature of ion-beam-defined wire arrays is strongly supported by the results of the following experiment in which a field-effect gate was used to tune the electronic widths of the wires. The field-effect gate consists of 7-nm-thick semitransparent NiCr and is evaporated on an ion-beam-defined wire array. The photoresist mask used for the ion-beam definition of the array is not removed before the evaporation process so that directly above the electron wires the distance of the metal gate is enlarged by the photoresist stripes. The gate is biased with respect to the electron wires. With this gate geometry the electron wires are effectively squeezed to smaller widths at negative gate voltages.[19] Since the electrons are pushed away from the ion-beam-defined boundaries we expect a gradual transition from rough ion-beam-defined to smooth field-effect-defined channel boundaries with a corresponding modification of the resonance linewidth.

Differential transmission spectra of a sample recorded at different gate voltages and at $B=0$ are depicted in Fig. 7. The photoresist grating has a period of $a=700$ nm. The heterojunction material used here is different from the one used for the other FIR investigations because here the barrier material between electron system and Schottky gate had to be optimized for the use of a depletion gate. The leakage current through the Schottky gate is drastically reduced in the sample of Fig. 7. Further wafer specifications are given in the caption of Fig. 7. The resonance linewidth at gate voltage $V_g=0$ is 6.2 cm^{-1} and it clearly reduces by a factor of two to 3.1 cm^{-1} at $V_g=-200$ mV and roughly stays constant at lower gate voltages. At positive gate voltages the electrons enter into the ion-beam-irradiated areas and the linewidth increases accordingly. A characteristic change in the behavior of the resonance positions is observed at a positive gate voltage of $V_g=100$ mV. Whereas below this voltage the resonance position decreases with increasing

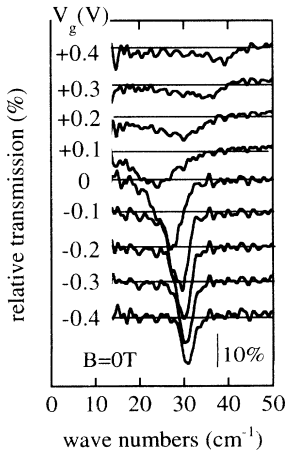

FIG. 7. Spectra of an electron wire array with $a=700$-nm period with an additional gate on top of the irradiation mask recorded at $T=2$ K. The gate voltages indicated are applied between the gate and the electron system. The heterojunction layer from which the wire array is fabricated has a mobility of 115 m^2/Vs, an electron density of 3.8×10^{15} m^{-2} at $T=4.2$ K and the electron system is 60 nm below the crystal surface.

gate voltage, it increases beyond 100 mV. Furthermore, at positive gate voltages above 200 mV in a magnetic field an additional resonance becomes observable at the cyclotron frequency, proving that the array of isolated electron wires has transformed into a 2DES.[19] We thus probe at $V_g > 100$ mV the cyclotron resonance and the plasmon excitation of a 2DES with density and—as we believe—mobility modulation.

The behavior of the resonance position is in close correspondence to observations on purely field-effect-defined electron wires.[19] There, a corresponding transition from a 2DES to an array of isolated wires is observed at negative gate voltages.[2,19] The resonance positions behave very similarly: At gate voltages above the transition point both a cyclotron resonance and a 2D-plasmon excitation are observed. The 2D-plasmon resonance frequency increases with increasing gate voltage reflecting the increasing average electron density. At lower gate voltages only the dimensional resonance is observed with a resonance position that increases with decreasing gate voltage reflecting the increasing curvature of the confinement potential.[51]

The behavior of the resonance widths in the ion-beam-defined wire arrays is characteristically different from the one in purely field-effect-defined arrays. There the 2D-plasmon linewidth is relatively small and increases with decreasing gate voltage, i.e., increasing density modulation. The FWHM broadens drastically in the 2D-1D-transition regime but quickly narrows once the wire array is formed. This has been attributed to Landau damping in the transition region.[52] At lower gate voltages the resonance linewidth increases with decreasing gate voltage which is explained in terms of potential fluctuations that are less effectively screened at reduced electron densities.[53] In contrast, in the ion-beam-defined wire arrays both the 2D plasmon as well as the cyclotron resonance in the 2D-gate-voltage regime above 100 mV are very broad. The dimensional resonance linewidth in the ion-beam-defined wire arrays decreases monotonically with decreasing gate voltage and finally stays constant at voltages below $V_g = -200$ mV. Although in this system the electron density is also reduced the FWHM decreases in the whole gate voltage range investigated because the electrons are squeezed away from the rough ion-beam-defined boundary. This indicates that at $V_g = 0$ V the linewidth is dominantly determined by the boundary scattering in ion-beam-defined wires.

The magnetic-field dependence of the resonance linewidth changes significantly with gate voltage. At $V_g = 0$ V the FWHM rises from 2 cm^{-1} at $B = 10$ T to 6.2 cm^{-1} at $B = 0$ T. With a negative gate voltage of -200 mV the linewidth only increases from 1.6 cm^{-1} at 10 T to 3.1 cm^{-1} at 0 T. As expected, the linewidth increase with decreasing magnetic field is much smaller at $V_g = -200$ mV, and is very similar to the behavior observed in purely field-effect-defined wire arrays.[19,49]

In the following we would like to discuss investigations of one-dimensional-intrasubband plasmons in electron wires. We find that the linewidth of the intrasubband plasmon is much less affected by the boundary roughness than the one of the intersubband plasmon. We investigated the intrasubband plasmon in wire arrays with period $a = 700$ nm. After successful ion-beam patterning a gold grating coupler was prepared on the surface of the crystal as described in Sec. II. This grating coupler with period $b = 1$ μm and oriented perpendicular to the electron wires serves to couple the FIR radiation to the longitudinal one-dimensional plasmon with corresponding wave vector $q = 2\pi/b$ along the wires.[21] With unpolarized FIR radiation we now observe in addition to the dimensional resonance an intrasubband plasmon as illustrated in Fig. 8. The positions of the resonances taken

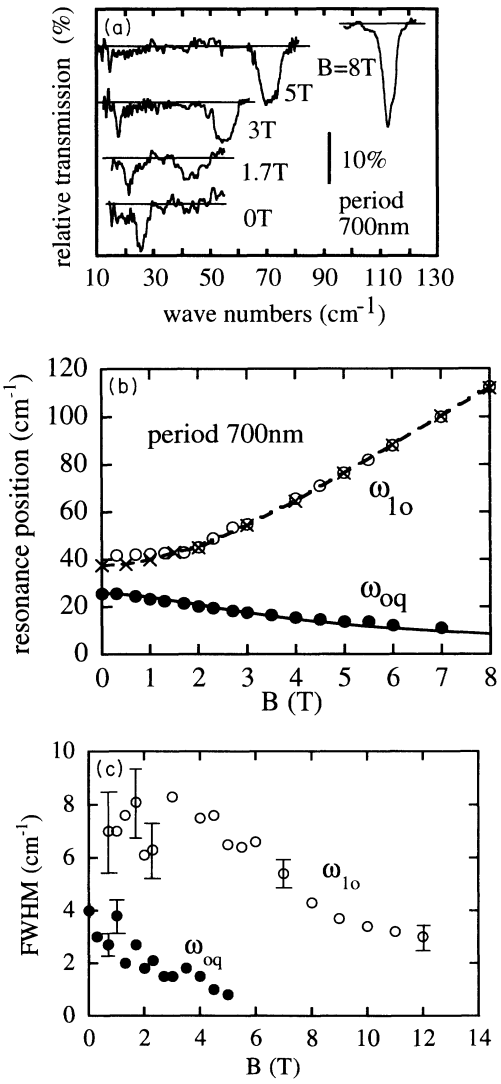

FIG. 8. (a) Typical FIR spectra at $T = 2$ K of an ion-beam-defined multiwire array with period 700 nm and an additional grating coupler with period 1 μm on the sample surface oriented perpendicular to the wire array. The electron wire array is prepared from the same heterojunction material as the sample in Fig. 5. (b) Resonance positions of the intersubband plasmons ω_{10} (open circles) and the intrasubband plasmons ω_{0q} (filled circles). Crosses denote resonance positions measured before the grating coupler was prepared on the sample surface. The solid and the dashed lines are calculated as described in the text. (c) Resonance linewidths of the ω_{0q}- (filled circles) and the ω_{10}-mode (open circles).

from the spectra of Fig. 8(a) are depicted in Fig. 8(b). Now two branches are observed, the high-frequency mode ω_{10} being the intersubband plasmon which had already been observed on the sample before preparation of the grating coupler. It is only slightly shifted with respect to the resonance positions measured without grating coupler. As indicated by the filled circles in Fig. 8(b) an additional low-frequency mode ω_{0q} is observed after preparation of the grating coupler. This mode has a negative magnetic-field dispersion, which is a characteristic property of intrasubband plasmons in one-dimensional electron systems.[21,50]

Before we discuss the magnetic-field dispersion of the resonance position we would like to focus on the resonance linewidths of the two modes as displayed in Fig. 8(c). The linewidth of the intersubband plasmon ω_{10} is roughly 7 cm^{-1} at $B=0$ and decreases to half that value at high magnetic fields. There is no significant difference in the linewidth behavior before and after grating coupler preparation. The most interesting feature obvious in Fig. 8(c) is that the resonance linewidth of the intrasubband plasmon ω_{0q} at $B=0$ is about half the value of the intersubband plasmon and decreases faster with increasing magnetic field so that at $B=5$ T the linewidth is six times smaller than the one of the ω_{10} mode.

This behavior can be understood qualitatively by considering the electron motion associated with the corresponding FIR modes. The intersubband resonance at zero magnetic field corresponds to an electron motion perpendicular to the boundaries of the wire so that the periodicity of the motion is very effectively destroyed by diffuse boundary scattering processes. On the other hand, the one-dimensional intrasubband excitation is associated with charge-density waves propagating along the wires. Hence, the corresponding electron trajectories are reflected at glancing angles from the boundaries and only those electrons moving in close vicinity to the wire boundary are scattered.

The difference between the linewidths of the intrasubband and the intersubband plasmons gets even larger in a magnetic field. This behavior might be considered surprising at first glance since the one-dimensional intrasubband plasmon becomes an edge-type mode with increasing magnetic field.[21,54] However, the behavior of the linewidth can be understood in close analogy to the behavior of the edge magnetoplasmon in electron dots. Actually, the character of the intrasubband plasmon is very similar to the edge-type mode of the dimensional resonance in electron dots at high magnetic fields.[54,55] In model calculations the resonance linewidth of the edge-type resonance can easily be shown to decrease with increasing magnetic field.[56,57] This can be understood in terms of the dependence of the resonance frequency and linewidth on the diagonal and nondiagonal components of the conductivity. In high magnetic fields the resonance frequency of the edge-type mode is proportional to the nondiagonal component of the conductivity whereas the damping is proportional to the diagonal component.[57] Furthermore, the diagonal conductivity component is strongly reduced in high magnetic fields, so that the charge density built up at the dot perimeter circulates around the dot without significant damping. We note, that in ion-beam-defined electron dot matrices we observe dimensional resonances where the linewidth of the low-frequency mode also decreases significantly with increasing magnetic field.

In the following we briefly discuss the resonance positions in Fig. 8(b). One-dimensional plasmons have been studied theoretically in different limits with respect to the wire width and separation as compared to the plasmon wavelength.[50,58,59] In our case the plasmon wavelength is comparable to the wire width and the wire separation is so large that the interaction effects between adjacent wires are expected to be small. Then the plasmon frequency at $B=0$ can be approximated by[50]

$$\omega_{nq}^2=\frac{n_s e^2}{2\varepsilon\varepsilon_0 m^*}\left[\left[\frac{n\pi}{W}\right]^2+q^2\right]^{1/2}. \tag{1}$$

Here ε is the effective dielectric constant of the material in which the electron system is embedded, m^* is the effective mass, W the width of the wire, and n_s an effective areal electron density within the channel. This formula, basically, is derived from the dispersion of a plasmon in a 2DES with a wave vector given by the term in the square bracket. Like in a wave guide this wave vector is determined by the mode distribution across and the wave vector $q=2\pi/b$ along the channel. Relation (1) was previously found to describe the behavior of intrasubband plasmons investigated in electron wires fabricated by etching techniques.[21,60]

According to Eq. (1) we can evaluate the effective wire width W in our sample from the ratio $\omega_{0q}^2/\omega_{10}^2=2W/b$. With the experimental values $\omega_{10}=38$ cm^{-1} and $\omega_{0q}=26$ cm^{-1} we get $W=230$ nm. This value compares well with the effective wire width extracted from comparison of the averaged areal electron density in the wire array with the electron density of the unprocessed wafer material. The averaged areal density can be evaluated from the oscillator strength at high magnetic field before grating gate preparation. Assuming that the effective 2D electron density within the wires does not change when the wires are defined, we derive from the ratio of densities an approximate effective wire width of 230 nm$\pm$20%. From inspection with a scanning electron microscope we determine a photoresist stripe width of 280 nm$\pm$10%. The corresponding sidewall depletion length as evaluated from these experiments is 25 nm, which is in accordance with the previous finding in Sec. III. Our analysis with Eq. (1) neglects a possible coupling between the two modes, which might exist if the high-frequency mode had a q-dependent part. Eventually a weak coupling could explain the slight deviation of the high-frequency mode observed in Fig. 8(b) before and after preparation of the grating coupler.

The magnetic field dispersions of the modes are well described by the dashed and the full lines in Fig. 8(b), respectively. Again the dashed line is calculated according to the formula $\omega_{\rm res}^2=\omega_{10}^2+\omega_c^2$, with $\omega_{10}=38$ cm^{-1}. The full line through the positions of the intrasubband plasmon ω_{0q} is calculated according to

$$\omega_{0q}^2(B\neq 0)=\omega_{0q}^2(B=0)\frac{\omega_{10}^2}{\omega_{10}^2+\omega_c^2} . \quad (2)$$

Here the magnetic field dispersion of the intrasubband plasmon is assumed to arise solely from a renormalization of the effective mass m^* in Eq. (1) in close analogy to an argument used by Wixforth *et al.*[61] for the description of the intrasubband plasmon in a wide parabolic quantum well in a parallel magnetic field. We assume the electrons to move in a parabolic bare potential with a characteristic frequency ω_{10}, so that for the free electron motion along the wires the energy is $p^2/2m^*(B)$, where p is the electron momentum and the mass is renormalized according to $m^*(B)=m^*(\omega_{10}^2+\omega_c^2)/\omega_{10}^2$.

V. CONFINEMENT MECHANISM

The FIR measurements described above were recorded when the samples were carefully shielded from radiation with wavelengths shorter than the far infrared. In Fig. 9 we show the behavior of the FIR resonances of a multiwire array with period 500 nm after a few minutes' illumination with a red light-emitting diode at low temperatures. The sample of this figure is the same as the one of Figs. 5 and 6. The resonance positions after the illumination do not deviate from the cyclotron resonance frequency anymore. The resonance linewidth now is large in the whole magnetic-field region investigated. We infer that at least those parts of the confinement potential have been lifted by the illumination that lead to a dimensional resonance shifted from the cyclotron frequency. The scattering centers, on the other hand, have not been completely removed, if their number is reduced at all. After annealing this sample at 400 °C in Ar/H_2 atmosphere the linewidth measured, e.g., at 3 T decreases from 18 to 3 cm^{-1}, while the absorption amplitude increases from 2% to 35%. From this we infer that the confinement potential as well as most of the mobility reducing defects are removed by the annealing process.

In order to improve our understanding of the confinement mechanism in the ion-beam patterning technique we also performed luminescence studies. In Fig. 10

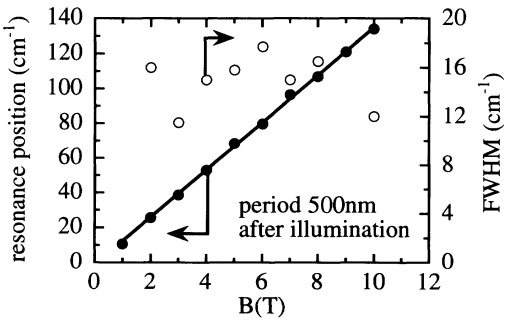

FIG. 9. FIR-resonance positions (filled circles) and FWHM (open circles) of the sample in Fig. 5 after illumination with a short pulse of a red light-emitting diode recorded at $T=2$ K. The solid line represents the cyclotron frequency.

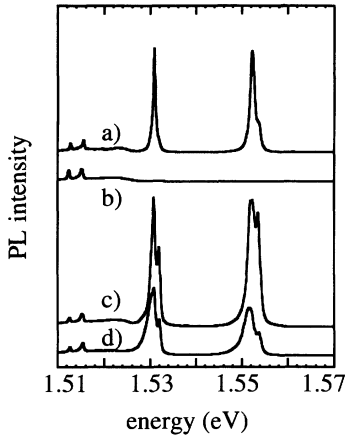

FIG. 10. Photoluminescence spectra ($T=10$ K) of an undoped double quantum-well structure (10 and 15 nm wide, 70 and 100 nm below the surface, respectively) after exposure to an ion dose typical for patterning. (a) Spectrum with the laser spot ($E=2.41$ eV) focused on a part which has been protected by a mask during irradiation. (b) Spot on the unprotected area. (c) and (d) are spectra from the sample after an additional annealing step (500 °C). (c) and (d) are recorded on the same sample parts as (a) and (b), respectively.

we present photoluminescence (PL) spectra of an undoped $Al_xGa_{1-x}As/GaAs$ (with $x=0.35$) double-quantum-well structure that has been irradiated with an ion dose of 5 mC/cm^2. This is a typical dose used in the above samples for successful patterning of a 2DES. The quantum wells are located 70 and 100 nm below the surface and are 10 and 15 nm wide, respectively. The luminescence is excited with a laser beam ($E=2.41$ eV) focused on different parts of the sample when the spectra (a) and (b) were recorded. The top spectrum (a) has been recorded with the laser spot on a part of the sample which had been protected by a photoresist mask during irradiation. The spectrum taken in the protected part is not changed by the irradiation. The spectrum (b) was recorded with the spot focused on the unprotected area. The spectra are scaled to give a constant intensity of the GaAs-substrate peaks (around 1.515 eV), that should hardly be affected by the irradiation. In comparison, the PL of the quantum wells is quenched completely. Obviously, the photoexcited carriers recombine nonradiatively at defects that have been created by the ion-beam-irradiation at the location of the quantum well. After an additional anneal in Ar/H_2 at 500 °C the PL measured on the ion-beam-exposed parts of the sample recovers [Fig. 10(d)] and gets similar in intensity and line shape to the PL measured on the part of the sample having been protected by resist during exposure [Fig. 10(c)]. We note that the latter has changed slightly after the annealing step. The dc conductivity of a homogeneously irradiated unmasked modulation-doped $Al_xGa_{1-x}As/GaAs$ structure also shows a substantial mobility reduction caused by defects created during the irradiation near the location of the 2DES.

Above results give valuable information about the

mechanism that leads to the lateral confinement in ion-beam-patterned $Al_xGa_{1-x}As/GaAs$ heterojunctions. Simulations with the Monte Carlo program TRIM (Ref. 17) show that the average range of Neon ions with an energy of 300 eV in GaAs is only a few nanometers, assuming channeling effects to be neglected. The electron system is typically 50 to 100 nm below the surface. However, in our photoluminescence data (Fig. 10) we demonstrate that defects are created at the quantum well located 100 nm below the crystal surface. With a small magnet and an aperture we have made a charge analysis of the ion plasma in our ion-milling chamber. A significant fraction of the Ne ions are double or triple ionized. A numerical simulation by Stoffel[18] for Ar ions shows that double ionized Ar ions with an energy of 1 keV can reach the depth of the electron system by a process similar to "channeling." Thus, a fraction of the Ne ions may reach the interface of the heterostructure in our samples. From the doses used to pattern the electron system we estimate that about 10^4-10^5 Neon ions are necessary to remove or at least localize one mobile electron in the irradiated area, so that even a very small fraction of the incident dose still is a considerable number of ions in comparison to the electrons in the 2DES. Our experimental results indicate, that the confinement potential consists of two different parts. A long-range potential determines the FIR-resonance frequency within the wire and can be removed by illumination. A short-range potential causes a severe mobility reduction in the ion-exposed areas as well as diffuse scattering at the boundaries between exposed and protected areas. This potential persists when the sample is illuminated, but can be reduced by an anneal step.

VI. CONCLUSION

We have studied electron systems laterally patterned by low-energy ion-beam irradiation. This technique is barely accompanied with material removal from the surface and thus well suited for combination with other patterning techniques such as field-effect gates or grating couplers. The magnetotransport data demonstrate that ion-beam-defined boundaries are very rough in the sense that they scatter the electrons diffusely—a finding that is in agreement with previously published results on electron wires fabricated with this technique. The ion-beam-irradiation technique thus enables us to study how the rough boundaries affect the high-frequency conductivity in electron wires. We investigate in the FIR one-dimensional-intersubband as well as intrasubband plasmons. It is found that the linewidth of the intersubband plasmon or dimensional resonance drastically broadens with decreasing wire width and narrows if a high magnetic field is applied perpendicular to the wires. From this we infer that the linewidth of this excitation in ion-beam-defined wire arrays is strongly affected by the rough wire boundaries. In contrast, the linewidth of the intrasubband plasmon is found to be significantly smaller than the linewidth of the dimensional resonance. This is qualitatively explained with an anisotropic sensitivity of these modes on the specific form of the wire boundaries. We argue that intrasubband and intersubband plasmons are predominantly associated with charge propagating along and perpendicular to the wires, respectively, and that the electron motion along the channels is less affected by the rough boundaries than the perpendicular one.

We also discuss photoluminescence studies on a $Al_xGa_{1-x}As/GaAs$ double quantum-well structure having been exposed to a low-energy ion beam. From the complete disappearance of the luminescence we infer that the irradiation process creates defects near the location of the quantum well, at which photoexcited carriers recombine nonradiatively. This verifies that defects are created far below the crystal surface, although at the ion energies used here the penetration depth of almost all ions is predicted to be only several nanometers. Experiments on samples having been illuminated with red light verify that these defects can seriously deteriorate the electron mobility in the ion-beam-exposed areas. The transport experiments suggest that these defects also cause the boundaries of the patterned electron systems to scatter diffusely.

ACKNOWLEDGMENTS

We thank H. Drexler, A. Huber, S. A. Mikhailov, M. Suhrke, and A. Wixforth for very valuable discussions and gratefully acknowledge financial support by the Deutsche Forschungsgemeinschaft.

[1]For a review see, *Nanostructured Systems,* in Semiconductors and Semimetals Vol. 35, edited by R. K. Williardson, A. C. Beer, E. R. Weber, and M. Reed (Academic, San Diego, 1992).

[2]W. Hansen, U. Merkt, and J. P. Kotthaus, in *Nanostructured Systems,* Semiconductors and Semimetals Vol. 35, edited by R. K. Williardson, A. C. Beer, E. R. Weber, and M. Reed (Acacdemic, San Diego, 1992), p. 279.

[3]H. Z. Zheng, H. P. Wei, D. C. Tsui, and G. Weimann, Phys. Rev. B **34**, 5635 (1986).

[4]K.-F. Berggren, T. J. Thornton, D. J. Newson, and M. Pepper, Phys. Rev. Lett. **57**, 1769 (1986).

[5]S. E. Laux, D. J. Frank, and F. Stern, Surf. Sci. **196**, 101 (1988).

[6]A. Kumar, S. E. Laux, and F. Stern, Appl. Phys. Lett. **54**, 1270 (1989).

[7]D. A. Wharam, U. Ekenberg, M. Pepper, D. G. Hasko, H. Ahmed, J. E. F. Frost, D. A. Ritchie, D. C. Peacock, and G. A. C. Jones, Phys. Rev. B **39**, 6283 (1989).

[8]M. L. Roukes, A. Scherer, S. J. Allen, Jr., H. G. Craighead, R. M. Ruthen, E. D. Beebe, and J. P. Harbison, Phys. Rev. Lett. **59**, 3011 (1987).

[9]C. W. J. Beenakker and H. van Houten, Phys. Rev. B **37**, 6544 (1988).

[10]C. W. J. Beenakker and H. van Houten, Phys. Rev. B **38**, 3232 (1988).

[11]T. J. Thornton, M. L. Roukes, A. Scherer, and B. P. Van der

Gaag, Phys. Rev. Lett. **63**, 2128 (1989).
[12]A. Scherer, M. L. Roukes, H. G. Craighead, R. M. Ruthen, E. D. Beebe, and J. P. Harbison, Appl. Phys. Lett. **51**, 2133 (1987).
[13]A. Scherer and M. L. Roukes, Appl. Phys. Lett. **55**, 377 (1989).
[14]T. J. Thornton, M. L. Roukes, A. Scherer, and B. P. van der Gaag, in *Science and Engineering of 1- and 0-Dimensional Semiconductors,* edited by S. P. Beaumont and C. M. Sottomayor-Torres (Plenum, New York, 1990), p. 25.
[15]T. L. Cheeks, M. L. Roukes, A. Scherer, and H. G. Craighead, Appl. Phys. Lett. **53**, 1964 (1988).
[16]M. A. Foad, S. Thoms, and C. D. W. Wilkinson, J. Vac. Sci. Technol. B **11**, 20 (1993).
[17]J. F. Ziegler, J. P. Biersack, and U. Littmark, *The Stopping and Range of Ions in Solids* (Pergamon, New York, 1985).
[18]N. G. Stoffel, J. Vac. Sci. Technol. B **10**, 651 (1992).
[19]W. Hansen, M. Horst, J. P. Kotthaus, U. Merkt, Ch. Sikorski, and K. Ploog, Phys. Rev. Lett. **58**, 2586 (1987).
[20]T. Demel, D. Heitmann, P. Grambow, and K. Ploog, Phys. Rev. B **38**, 12 732 (1988).
[21]T. Demel, D. Heitmann, P. Grambow, and K. Ploog, Phys. Rev. Lett. **66**, 2657 (1991).
[22]Y. Ochiai, T. Onishi, J. P. Bird, M. Kawabe, K. Ishibashi, Y. Aoyagi, and S. Namba, Surf. Sci. **263**, 388 (1992).
[23]R. J. Blaikie, K. Nakazato, J. R. A. Cleaver, and H. Ahmed, Phys. Rev. B **46**, 9796 (1992).
[24]H. van Houten, B. J. van Wees, M. G. J. Heijman, and J. P. Andre, Appl. Phys. Lett. **49**, 1781 (1986).
[25]H. van Houten, B. J. van Wees, J. E. Mooij, G. Roos, and K.-F. Berggren, Superlatt. Microstruct. **3**, 497 (1987).
[26]A. M. Chang, G. Timp, T. Y. Chang, J. E. Cunningham, P. M. Mankiewich, R. E. Behringer, and R. E. Howard, Solid State Commun. **67**, 769 (1988).
[27]Y. Takagaki, K. Gamo, S. Namba, S. Ishida, S. Takaoka, and K. Murase, J. Appl. Phys. **67**, 340 (1990).
[28]S. Takaoka, K. Tsukagoshi, K. Oto, T. Sawasaki, K. Murase, Y. Takagaki, K. Gamo, and S. Namba, Surf. Sci. **267**, 282 (1992).
[29]K. Ishibashi, Y. Aoyagi, S. Namba, Y. Ochiai, J. P. Bird, and M. Kawabe, Surf. Sci. **263**, 378 (1992).
[30]E. Ditlefsen and J. Lothe, Philos. Mag. **14**, 759 (1966).
[31]S. Block, M. Suhrke, S. Wilke, A. Menschig, H. Schweizer, and D. Grützmacher, Phys. Rev. B **47**, 6524 (1993).
[32]K. K. Choi, D. C. Tsui, and K. Alavi, Appl. Phys. Lett. **50**, 110 (1987).
[33]T. Demel, D. Heitmann, P. Grambow, and K. Ploog, Appl. Phys. Lett. **53**, 2176 (1988).
[34]J. F. Weisz and K.-F. Berggren, Phys. Rev. B **40**, 1325 (1989).
[35]F. Brinkop, W. Hansen, J. P. Kotthaus, and K. Ploog, Phys. Rev. B **37**, 6547 (1988).
[36]J. H. English, A. C. Gossard, H. L. Störmer, and K. W Baldwin, Appl. Phys. Lett. **50**, 1826 (1987).
[37]P. A. Lee and A. D. Stone, Phys. Rev. Lett. **55**, 1622 (1985).
[38]M. Wendel, C. Lettau, W. Hansen, V. Dolgopolov, G. Böhm, and G. Weimann, Solid State Commun. **87**, 1101 (1993).
[39]A. M. Chang, T. Y. Chang, and H. U. Baranger, Phys. Rev. Lett. **63**, 996 (1989).
[40]C. J. B. Ford, S. Washburn, M. Büttiker, C. M. Knoedler, and J. M. Hong, Phys. Rev. Lett. **62**, 2724 (1989).
[41]M. L. Roukes, A. Scherer, and B. P. Van der Gaag, Phys. Rev. Lett. **64**, 1154 (1990).
[42]C. W. J. Beenakker and H. van Houten, Phys. Rev. Lett. **60**, 2406 (1988).
[43]C. W. J. Beenakker and H. van Houten, Phys. Rev. Lett. **63**, 1857 (1989).
[44]H. U. Baranger and A. D. Stone, Phys. Rev. Lett. **63**, 414 (1989).
[45]T. Geisel, R. Ketzmerick, and O. Schedletzky, Phys. Rev. Lett. **69**, 1680 (1992).
[46]E. Batke and D. Heitmann, Infrared Phys. **24**, 189 (1984).
[47]H. Drexler, W. Hansen, J. P. Kotthaus, M. Holland, and S. P. Beaumont, Phys. Rev. B **46**, 12 849 (1992).
[48]Q. P. Li and S. Das Sarma, Phys. Rev. B **44**, 6277 (1991).
[49]W. Hansen, J. P. Kotthaus, A. Chaplik, and K. Ploog, in *High Magnetic Fields in Semiconductor Physics,* edited by G. Landwehr, Springer Series in Solid-State Sciences Vol. 71 (Springer, Heidelberg, 1987), p. 266.
[50]G. Eliasson, J.-W. Wu, P. Hawrylak, and J. J. Quinn, Solid State Commun. **60**, 41 (1986).
[51]W. Hansen, in *Physics of Nanostructures,* edited by J. H. Davies and D. A. Long (Scottish Universities Summer School in Physics and Institute of Physics Publishing, Bristol, 1992), p. 257.
[52]C. Dahl, Phys. Rev. B **41**, 5763 (1990).
[53]J. A. Nixon and J. H. Davies, Phys. Rev. B **41**, 7929 (1990).
[54]A. L. Fetter, Phys. Rev. B **33**, 3717 (1986).
[55]A. L. Fetter, Phys. Rev. B **33**, 5221 (1986).
[56]B. A. Wilson, S. J. Allen, Jr., and D. C. Tsui, Phys. Rev. B **24**, 5887 (1981).
[57]S. A. Mikhailov, Pis'ma Zh. Eksp. Teor. Fiz. **57**, 570 (1993) [JETP Lett. **57**, 587 (1993)].
[58]S. Das Sarma and W. Lai, Phys. Rev. B **32**, 1401 (1985).
[59]A. Gold, Z. Phys. B **89**, 213 (1992).
[60]T. Egeler, G. Abstreiter, G. Weimann, T. Demel, D. Heitmann, P. Grambow, and W. Schlapp, Phys. Rev. Lett. **65**, 1804 (1990).
[61]A. Wixforth, M. Kaloudis, M. Sundaram, and A. C. Gossard, Solid State Commun. **84**, 861 (1992).